LA-UR- 96-3954

CONF-970233--2

Author(s): Scott W. Doebling, ESA-EA, LANL
Charles R. Farrar, ESA-EA, LANL
Randall S. Goodman, University of Colorado*
*Formally UGS, ESA-EA

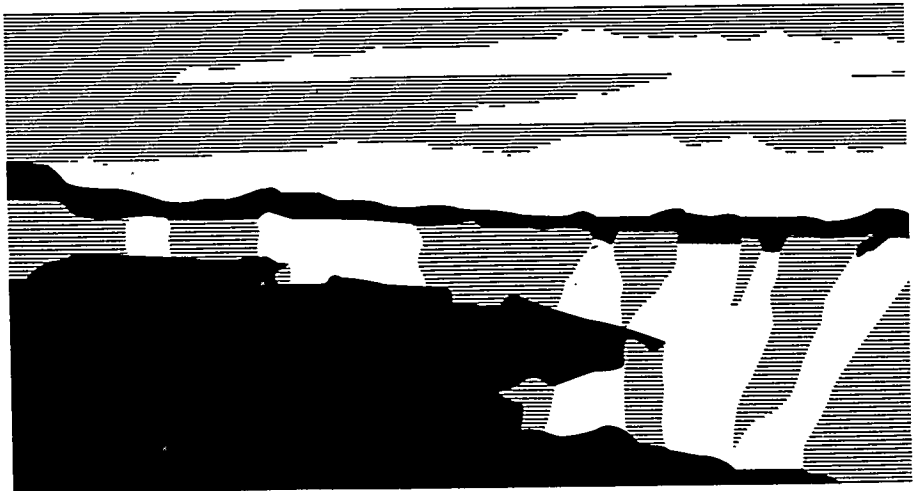DISTRIBUTION OF THIS DOCUMENT IS UNLIMITED

MASTER

Los Alamos
NATIONAL LABORATORY

DISCLAIMER

DISCLAIMER

Portions of this document may be illegible
in electronic image products. Images are
produced from the best available original
document.

EFFECTS OF MEASUREMENT STATISTICS ON THE DETECTION OF DAMAGE IN THE ALAMOSA CANYON BRIDGE

Scott W. Doebling[1], Charles R. Farrar[2]
Los Alamos National Laboratory
Los Alamos, NM, 87545

Randall S. Goodman[3]
University of Colorado
Boulder, CO, 80309

ABSTRACT

This paper presents a comparison of the statistics on the measured modal parameters of a bridge structure to the expected changes in those parameters caused by damage. It is then determined if the changes resulting from damage are statistically significant. This paper considers the most commonly used modal parameters for indication of damage: modal frequency, mode shape, and mode shape curvature. The approach is divided into two steps: First, the relative uncertainties (arising from random error sources) of the measured modal frequencies, mode shapes, and mode shape curvatures are determined by Monte Carlo analysis of the measured data. Based on these uncertainties, 95% statistical confidence bounds are computed for these parameters. The second step is the determination of the measured change in these parameters resulting from structural damage. Changes which are outside the 95% bounds are considered to be statistically significant. It is proposed that this statistical significance can be used to selectively filter which modes are used for damage identification. The primary conclusion of the paper is that the selection of the appropriate parameters to use in the damage identification algorithm must take into account not only the sensitivity of the damage indicator to the structural deterioration, but also the uncertainty inherent in the measurement of the parameters used to compute the indicator.

INTRODUCTION

Damage identification using changes in measured modal parameters is a topic that has received considerable attention in the literature in recent years. A review of the state of the art in the field is presented in Ref. [1]. The majority of existing methods use the following three modal parameters as basic building blocks for damage identification: modal frequency, mode shape, and mode shape curvature. Frequency and mode shape are used in flexibility analysis (see Toksoy and Aktan [2]) and model correlation approaches (see Hemez and Farhat [3], Zimmerman and Kaouk [4], and Doebling [5]). Mode shape curvature is used primarily in discretized strain energy methods (see Stubbs, et al. [6]).

Each of these basic parameters has pros and cons for use in damage identification: The modal frequency has the advantage of ease and accuracy of measurement, but is not spatially specific and is not very sensitive to damage. The mode shape has the advantage of being spatially specific, but requires more sensors to measure and is more mathematically involved to extract from the data. The mode shape curvature offers spatial specificity along with high sensitivity to damage, but can be subject to numerical estimation difficulties resulting from the need for differentiation.

One characteristic of the basic modal damage indicators that is often overlooked is the statistical uncertainty inherent in the measurements caused by random variation in the signal. This uncertainty describes the amount by which one would expect the estimated value to change from one measurement to the next as a result of electrical noise, slight variations in testing conditions, environmental effects (such and temperature and wind), etc. Once the uncertainty bounds for each of the basic indicators has been defined, any change within that bound can be classified as "statistically insignificant," i.e. it can be attributed to the random variations. Thus, the statistical uncertainty on the damage indicators must be defined so that the analyst can determine whether an observed

---

change in the indicator is large enough to be indicative of damage, or whether it can be attributed to the natural variations in the measurements.

In this paper, modal measurements from the Alamosa Canyon Bridge are analyzed to determine the 95% statistical uncertainty bounds on the modal frequencies, mode shapes, and mode shape curvatures. These uncertainty bounds are based on the propagation of standard values for the random error on the frequency response function (FRF) estimates through the modal identification procedure to the modal parameters.

Changes in the modal frequencies, mode shapes, and mode shape curvatures that are expected as a result of damage are computed using a correlated finite element model (FEM). These predicted changes are compared to the 95% confidence bounds computed from the experimental data, to determine which changes can be classified as statistically significant. A comparison is made of the overall statistical significance of the three indicators. The results indicate that although frequency is not very sensitive to damage, it has such low uncertainty bounds that it is a good indicator for the existence (not location) of the damage case considered. Also, particular components of the mode shape, and especially the mode shape curvature, can be statistically significant indicators of the location damage. However, the overall average values of the mode shape and mode shape curvature changes are typically not statistically significant.

EXPERIMENTAL TESTBED AND DATA ACQUISITION

The Alamosa Canyon Bridge has seven independent spans with a common pier between successive spans. An elevation view of the bridge is shown in Figure 1. The bridge is located on a seldom-used frontage road parallel to Interstate 25 about 10 miles North of the town of Truth or Consequences, New Mexico. Each

Figure 1. Elevation View of Alamosa Canyon Bridge

span consists of a concrete deck supported by six W30x116 steel girders. The roadway in each span is approximately 7.3 m (24 ft) wide and 15.2 (50 ft) long. Integrally attached to the concrete deck is a concrete curb and concrete guard rail. Inspection of the bridge showed that the upper flanges of the beams are imbedded in the concrete. Between adjacent beams are four sets of cross braces equally spaced along the length of the span. The cross braces are channel sections (C12x25). A cross section of the span at a location showing the interior cross braces is shown in Figure 2. At the pier the beams rest on rollers, and at the abutment the beams are bolted to a half-roller to approximate a pinned connection. These end conditions are shown in Figure 3.

The data acquisition system used in the vibration tests consisted of a Toshiba TECRA 700 laptop computer, four Hewlett Packard (HP) 35652A input modules that provide power to the accelerometers and perform analog to digital conversion of the accelerometer signals, an HP 35651A signal processing module that performs the needed fast Fourier transform calculations, and a commercial data acquisition/signal analysis software package produced by HP. A 3500 watt GENERAC Model R-3500 XL AC generator was used to power this system.
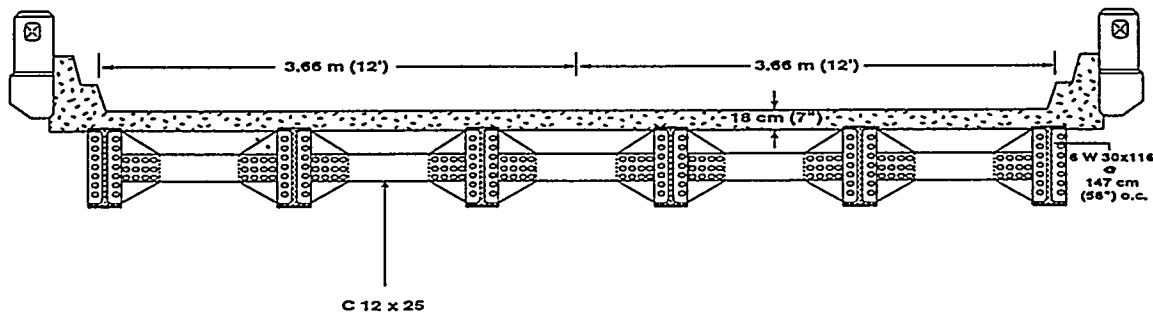

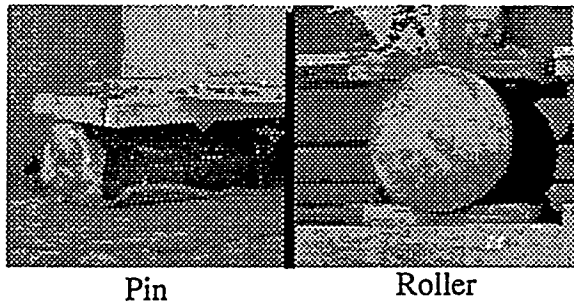Figure 2. Cross-Section of Alamosa Canyon Bridge Span

Pin   Roller

Figure 3. End Conditions of Alamosa Canyon Bridge Span

Figure 4. Accelerometer and Impact Locations

The data acquisition system was set up to measure acceleration and force time histories and to calculate FRFs, power spectral densities (PSDs), cross-power spectra and coherence functions. Sampling parameters were specified that calculated the FRFs from a 16-s time window discretized with 2048 samples. The FRFs were calculated for a frequency range of 0 to 50 Hz at a frequency resolution of 0.0625 Hz. A Force window was applied to the signal from the hammer's force transducer and exponential windows were applied to the signals from the accelerometers. AC coupling was specified to minimize DC offsets.

A PCB model 086B50 impact sledge hammer was used as the impact excitation source. The hammer weighed approximately 53.4 N (12 lbs) and had a 7.6-cm-dia. (3-in-dia) steel head. This hammer has a nominal sensitivity of 0.73 mV/lb and a peak amplitude range of 5000 lbs. A Wilcoxon Research model 736T accelerometer was used to make the driving point acceleration response measurement adjacent to the hammer impact point. This accelerometer has a nominal sensitivity of 100 mV/g, a specified frequency range of 5 - 15,000 Hz, and a peak amplitude range of 50 g. PCB model 336c integrated circuit piezoelectric accelerometers were used for the vibration measurements. These accelerometers have a nominal sensitivity of 1 V/g, a specified frequency range of 1 - 2000 Hz, and an amplitude range of 4 g. More details regarding the instrumentation can be found in Ref. [7].

A total of 31 acceleration measurements were made on the concrete deck and on the girders below the bridge as shown in Figure 4. Five accelerometers were spaced along the length of each girder. Because of the limited number of data channels, measurements were not made on the girders at the abutment or at the pier. Two excitations points were located on the top of the concrete deck. Point A was used as the primary excitation location. Point B was used to perform a reciprocity check. The force-input and acceleration-response time histories obtained from each impact were subsequently transformed into the frequency domain so that estimates of the PSDs, FRFs, and coherence functions could be calculated. Thirty averages were typically
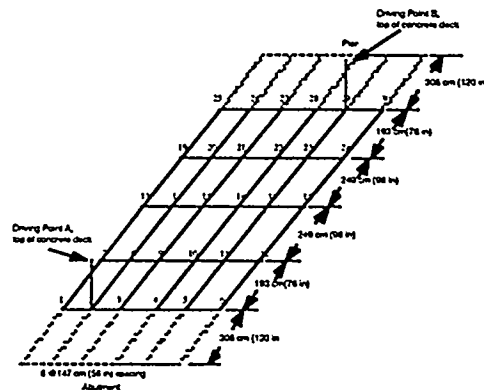
used for these estimates. With the sampling parameters listed above and the overload reject specified, data acquisition for a specific test usually occurred over a time period of approximately 30 - 45 minutes. All of the results in this paper are from measurements made on span 1 of the bridge, which is located at the far North end.

A total of 52 data sets were collected over the course of the six days of testing. Reciprocity and linearity checks were conducted first. A series of modal tests was conducted over a 24 hour period (one test every 2 hours) to assess the change in modal properties as a result of variations in ambient environmental conditions, as discussed in Ref. [7]. A series of tests with various levels of attempted damage was also conducted, but the permitted alterations in the bridge did not cause a significant change in the measured modal properties. Specifically, the nuts on the bolted connections that hold the channel-section cross members to the girders, as shown in Figure 5 were removed. However the bolts could not be loosened sufficiently, and no relative motion could be induced at the interface under the loading of the modal excitation. For this reason, the damage cases presented in this paper are results from simulated stiffness reduction using a correlated FEM.
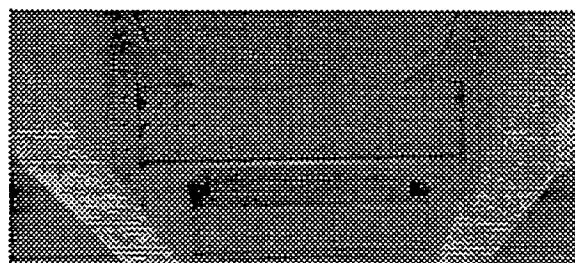

Figure 5. Bolted Connection of Cross-Member to Girder

MODAL IDENTIFICATION PROCEDURE

The first step in the analysis of the data was the determination of the approximate number of modes to be fit. This number was determined using the Multivariate Mode Indicator Function (MIF) [8] and the Complex Mode Indicator Function (CMIF) [9]. The MIF is an indication of how close to purely imaginary the response is at a particular frequency bin; thus frequencies which correspond to a peak in the MIF can be interpreted as possible modal frequencies. The values are normalized such that the MIF always falls between zero and one. The CMIF is a measure of the maximum singular values of the FRF matrix at each frequency bin. The CMIF also produces a peak at each modal frequency, but these peaks are proportional to the overall magnitude of the frequency response at that bin across all measured degrees of freedom (DOF). This proportionality is advantageous because it allows the user to get a feel for the relative strengths of each mode. However, it has the disadvantage that sometimes particularly strong modes can 'washout' nearby peaks. In this analysis, the CMIF and MIF were computed, and then zoomed to frequency bands of 10 Hz at a time. Approximately 9 modes of significant strength were located between 0 Hz and 30 Hz by inspection of the CMIF and MIF, as shown in Figure 6.
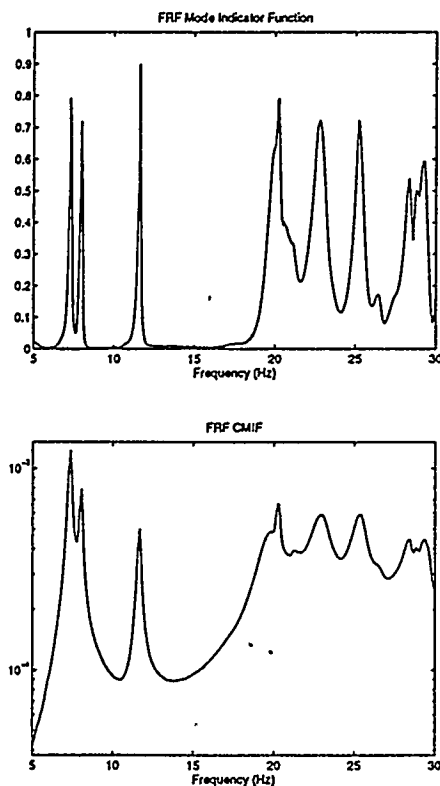

Figure 6. MIF and CMIF from Alamosa Canyon Bridge Data

The next step in the analysis was the application of ERA [10] to identify the modal frequencies, modal damping ratios, and mode shapes. The ERA procedure is based upon the formation of a Hankel matrix containing the measured discrete-time impulse response data, computed using the inverse fast Fourier transform of the measured FRFs. The shift in this matrix from one time step to the next is then used to estimate a discrete-time state space model for the structure. This data set contained 31 responses and 1 reference, and a Hankel matrix with 30 block rows and 200 block columns was used.

The model resulting from the ERA analysis had 80 modes, but it was known from examination of the MIF and CMIF that the data contains only about 9 modes in the band of interest. Thus it was necessary to apply some discrimination procedures to select the modes that were physically meaningful. There are three indicators developed specifically for use with ERA [11]: Extended Modal Amplitude Coherence (EMAC), Modal Phase Collinearity (MPC), and Consistent Mode Indicator (CMI), which is the product of EMAC and MPC. EMAC is a measure of how accurately a particular mode projects forward (in time) onto the impulse response data. MPC is a measure of how collinear the phases of the components of a particular complex mode are. If the phases are perfectly linear (i.e. either in phase or 180 degrees out of phase with each other), this mode is exactly proportionately damped, and can then be completely represented by a corresponding real mode shape. Thus, EMAC is a temporal quality measure and MPC is a spatial quality measure. Typically, we start with values of EMAC = 0.7, MPC = 0.7, and CMI = 0.5, and then see if all of the modes of interest (as determined by MIF and CMIF inspection) are preserved. In the current study, all 9 modes of interest passed this criteria, so these values of EMAC, MPC, and CMI were used as the cutoff values.

The next step in the process was visual inspection of the mode shapes. For a beam or plate-like structure, such as the Alamosa Canyon Bridge, the visual inspection of the mode shapes is particularly useful, because the response shapes are somewhat intuitive. The comparison of the measured modes to the FEM modes was useful as well, and a one-to-one correspondence was found between the 9 measured modes and 9 of the first 10 FEM modes. (One of the first 10 FEM modes was bending in the plane of the deck. This mode was not measured in this test because all of the sensors were perpendicular to the plane of the deck.)

The identified modal frequencies and modal damping ratios from this analysis are shown in Table 1. The mode shapes identified in this analysis are shown in Figure 7.

Table 1. Identified Modal Parameters from
Alamosa Canyon Bridge Test

Mode Number	Modal Frequency (Hz)	Modal Damping Ratio (%)
1	7.372	1.63%
2	8.043	1.84%
3	11.677	1.11%
4	20.191	0.57%
5	23.040	1.76%
6	25.448	1.92%
7	26.581	1.18%
8	27.637	2.04%
9	29.541	1.50%

STATISTICS ON MEASURED MODAL PARAMETERS

Statistical uncertainty bounds on the measured frequency response function magnitude and phase were computed from the measured coherence functions, assuming that the errors were distributed in a Gaussian manner, according to the following formulas from Bendat and Piersol [12]:

$$\sigma(|H(\omega)|) = \frac{\sqrt{1 - \gamma^2(\omega)}}{|\gamma(\omega)|\sqrt{2n_d}}|H(\omega)|$$

$$\sigma(\angle H(\omega)) = \frac{\sqrt{1 - \gamma^2(\omega)}}{|\gamma(\omega)|\sqrt{2n_d}}\angle H(\omega)$$

(1)

where $|H(\omega)|$ and $\angle H(\omega)$ are the magnitude and phase angle of the measured FRF, respectively, $\gamma^2(\omega)$ is the coherence function, n_d is the number of measurement averages, and $\sigma(\cdot)$ is the value of 1 standard deviation (68% uncertainty bound). These uncertainty bounds represent a statistical distribution of the FRF based on a realistic level of random noise on the measurement. Once the 1 standard deviation (68% uncertainty) bounds were known, 2 standard deviation (95% uncertainty) bounds were computed. Typical 95% uncertainty bounds on the FRF magnitude and phase for this data set are shown in Figure 8.

Statistical uncertainty bounds on the identified modal parameters (frequencies, damping ratios, and mode shapes) were estimated using the uncertainty bounds on the FRFs via a Monte Carlo analysis [13]. The basic idea of a Monte Carlo analysis is the repeated simulation of random input data, in this case the FRF with estimated mean and standard deviation values, and compilation of statistics on the output data, in

this case the ERA results. For this analysis, the procedure is summarized as:

1. Add Gaussian random noise to the FRFs using the noise standard deviations computed using Eq. (1). This additive noise represents a realistic level of random variations in the measurements.

2. Run the noisy FRF through the ERA identification procedure and apply the modal discrimination using the previously computed parameters.

3. Compute the mean and standard deviation of each modal frequency, damping ratio, and mode shape component over the total number of runs.

4. Repeat steps 1, 2, and 3 until the means and standard deviations calculated in step 3 converge.

For the current study, the convergence took about 100 runs. Tracking the convergence determined the sufficient sample size to provide significant confidence on the statistical estimates. The 95% uncertainty bounds on the modal frequencies, mode shapes, and mode shape curvatures resulting from random disturbances and noise, as computed by the Monte Carlo analysis, are presented in Table 2. It is observed from these results that the uncertainty bounds on the modal frequencies are much smaller than on the mode shapes, with the mode shape curvatures having the largest uncertainties. (The definition of the "average" errors for mode shape and mode shape curvature are presented in the comparison section of the paper.)

FINITE ELEMENT MODEL

Because the Alamosa Canyon Bridge consists of seven spans which are coupled only through the interaction of their expansion joints and the bridge piers, they were treated as independent so that only one span needed to be modeled. The FEM of 1 span of the Alamosa Canyon Bridge consisted of 612 thin shell elements for the bridge deck and 300 linear beam elements for the girders, cross members, and curbs. The guard rails were not included in the model. The full model had 990 nodes. The material and cross-sectional properties used in the model are shown in Table 3. The model was correlated with the measured modal frequencies from span 1 (far North end of the bridge) to improve the overall accuracy of its dynamic response. The material properties shown in Table 3 are the post-correlation values.

The boundary conditions of the bridge were originally intended to be pinned-roller connections, as shown in Figure 3. The original model contained sim-
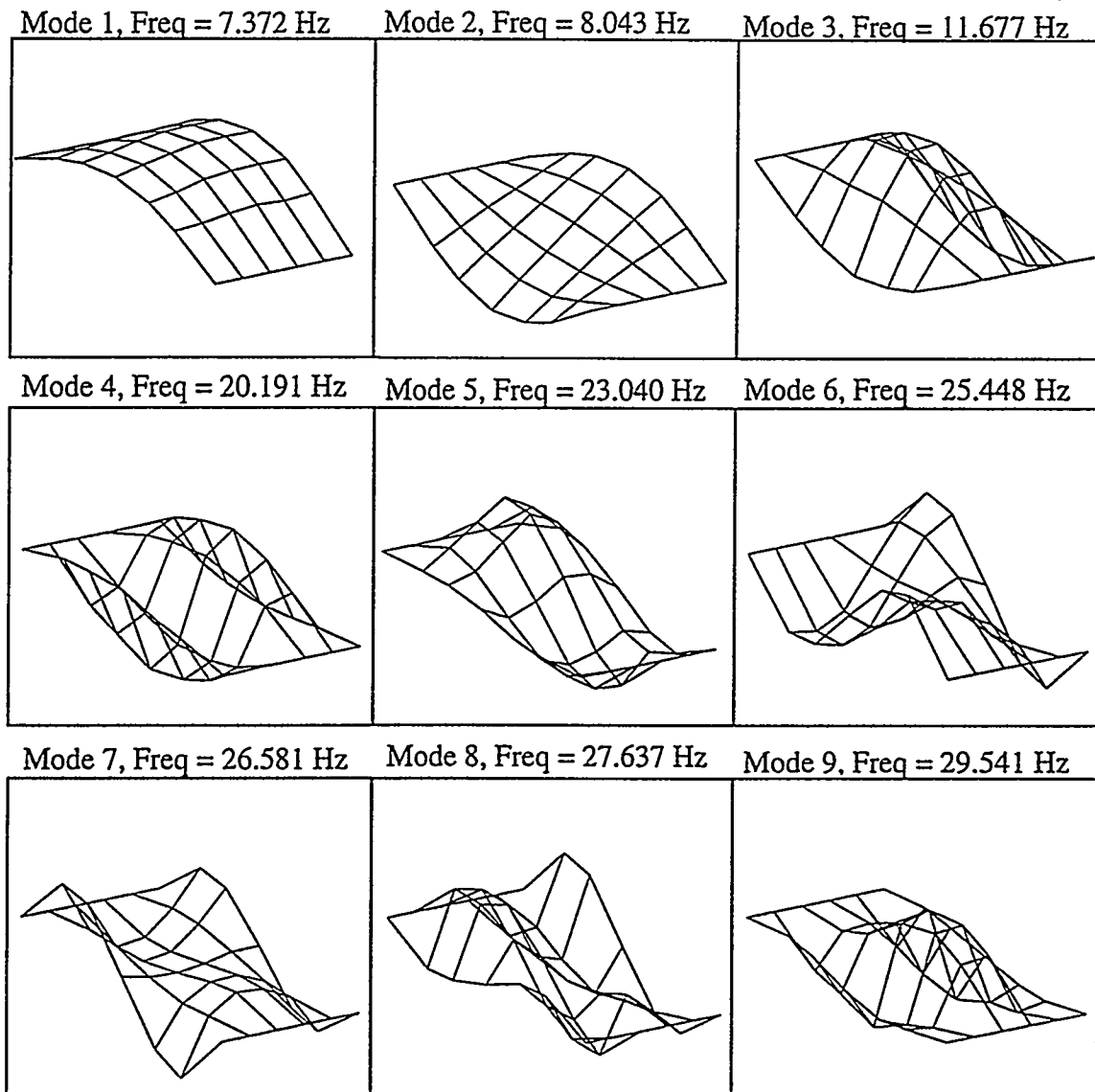
Mode 1, Freq = 7.372 Hz	Mode 2, Freq = 8.043 Hz	Mode 3, Freq = 11.677 Hz

Mode 4, Freq = 20.191 Hz	Mode 5, Freq = 23.040 Hz	Mode 6, Freq = 25.448 Hz

Mode 7, Freq = 26.581 Hz	Mode 8, Freq = 27.637 Hz	Mode 9, Freq = 29.541 Hz

Figure 7. Identified Mode Shapes for Alamosa Canyon Bridge

ple pin-rollers to simulate these end conditions. However, it was found that adding linear rotational springs to the pin connections improved the accuracy of the model.

Simulation of Damage

The damage case that was simulated for the Alamosa Canyon Bridge was the complete failure of the bolted connection of two cross members at an interior girder. This connection is shown in Figure 5. The damage was simulated by 99% reduction in the modulus of elasticity of the cross members on either side of the connection. Thus, their ability to carry loads is lost, but their mass is still contained in the model, as would be the case in an actual connection failure. The changes in the FEM modal frequencies, mode shapes, and mode

shape curvatures as a result of damage are presented in Table 4. It is observed in this table that the relative change of mode shapes is larger than that of frequencies, and the relative change of mode shape curvatures are typically the largest.

COMPARISON OF STATISTICS TO PREDICTED DAMAGE EFFECTS

A comparison of the estimated 95% confidence bounds and the predicted changes as a result of damage for the modal frequencies are shown in Figure 9. The modal frequencies of modes 3, 4, 7, 8, and 9 undergo a change that is significantly larger than the corresponding 95% confidence bounds. The relative magnitudes of the changes indicate that the frequency
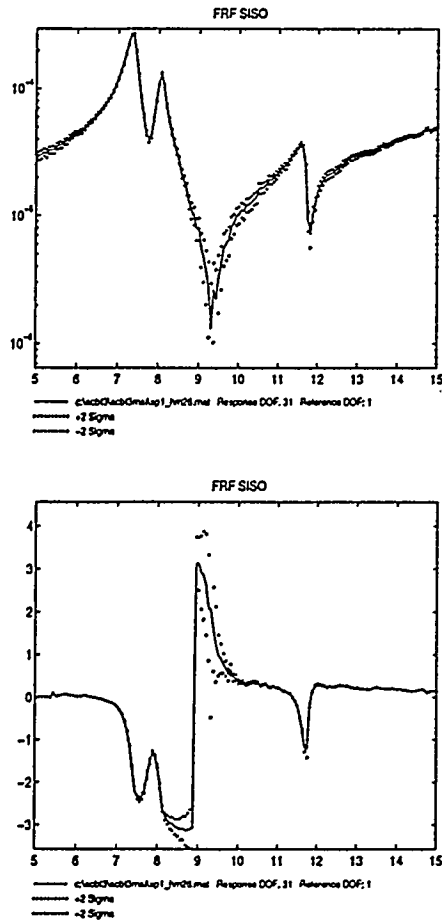
FRF SISO

FRF SISO

Figure 8. Typical 95% Confidence Bounds on FRF Magnitude and Phase

Table 2. Uncertainty Bounds on Measured Parameters from Random Disturbances

Mode #	Error on Modal Freq	Avg. Error on Mode Shape	Avg. Error on Mode Shape Curvature
1	0.06%	1.68%	555.49%
2	0.73%	45.42%	5118.41%
3	0.06%	1.74%	6.85%
4	0.24%	23.77%	12.98%
5	0.50%	157.83%	637.66%
6	0.06%	5.58%	36.97%
7	0.09%	3.63%	33.61%
8	0.11%	5.50%	9.54%
9	0.19%	156.16%	36.57%

Table 3. FEM Material and Cross-Sectional Properties

Name	Value
Modulus of Elasticity, Steel	30×10^6 psi
Density, Steel	7.32×10^{-4} $lb_f s^2/in^4$
Modulus of Elasticity, Concrete	3.012×10^6 psi
Density, Concrete	1.903×10^{-4} $lb_f s^2/in^4$
Cross Section, Girder	Wide Flange, W30X116
Cross Section, Cross Members	Channel, C12X25
Cross Section, Curb	Rectangle, 14 x 24

Table 4. Changes in FEM Modal Parameters Resulting From Damage

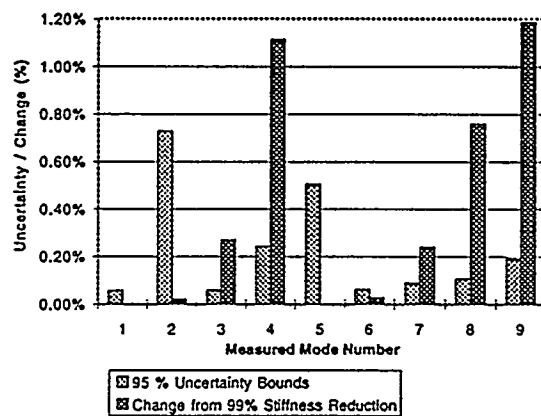| Mode Number	Change in Modal Freq	Avg. Change in Mode Shape	Avg. Change in Mode Shape Curvature
1	0.00%	0.03%	4.63%
2	0.02%	0.16%	2.35%
3	0.27%	0.87%	5.83%
4	1.11%	3.87%	3.49%
5	0.00%	0.07%	8.13%
6	0.03%	0.25%	1.78%
7	0.24%	1.49%	24.37%
8	0.76%	5.36%	6.49%
9	1.19%	20.65%	4.75%

Figure 9. Comparison of Modal Frequency 95% Confidence Bounds to Changes Predicted as a Result of Damage

changes of these modes could be used with confidence in a damage identification analysis. It should be noted from the y-axis scale of Figure 9 that the overall changes in frequency as a result of damage are quite small (< 1.2%), but as a consequence of the extremely low uncertainty bounds on the modal frequencies (many less than 0.2%), these small changes can be considered to be statistically significant.

One method for comparison of the confidence bounds on the mode shape components to the predicted change as a result of damage is a direct, component-by-component comparison. Such a comparison for modes 3 and 7 is shown in Figure 10. These plots show the
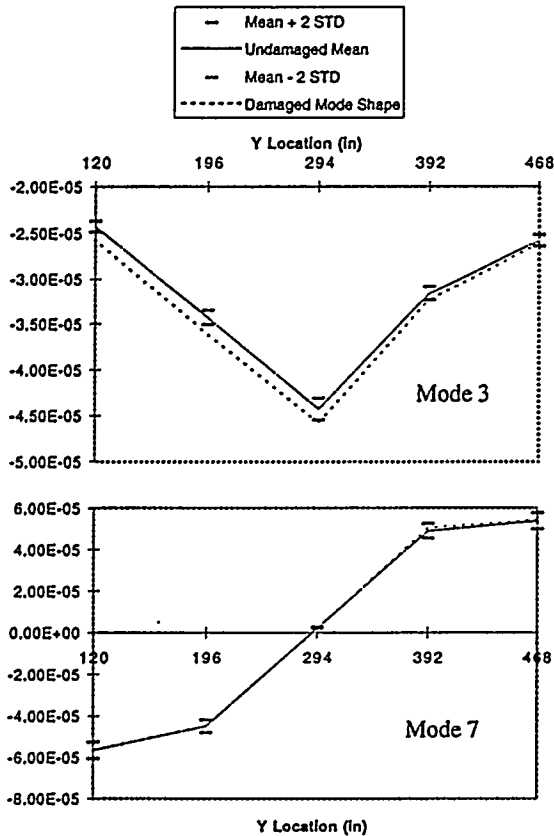

Figure 10. Comparison of Modes 3 and 7 Confidence Bounds and Predicted Change After Damage

mean values of the undamaged mode shape components in a solid line (with 95% confidence bounds at the measurement locations), with the predicted mode shape after damage represented by a dashed line. These mode shape components represent a "slice" of each of these mode shapes taken along one girder of the bridge. This slice of mode shape 3 contains 3 components that have a predicted change from damage that is greater than the 95% confidence bounds. Thus, the change in these 3 components can be used with confidence in a damage identification algorithm. How-

ever, none of the components of this slice of mode shape 7 have a change that is greater than the 95% bound, so these components of this mode shape have an insignificant change as a result of damage, and should not be used in a damage identification analysis.

An "average" of the component-by-component mode shape comparison shown above was computed to give an overall measure of the mode shape change and corresponding 95% confidence bound for each mode shape. The average mode shape change for mode j as a result of damage, $\overline{\Delta\phi}_j$, was defined as

$$\overline{\Delta\phi}_j = \frac{\sum_i (\phi_{ij}^d - \phi_{ij}^u)}{\sum_i |\phi_{ij}^u|} \qquad (2)$$

where ϕ_{ij} is the jth mode shape measured at the ith DOF, and the superscripts u and d refer to modes from the undamaged and damaged structure, respectively. A corresponding average 95% confidence bound for the jth mode, $\overline{\sigma}_j$, was defined as

$$\overline{\sigma}_j = \frac{2\sum_i \sigma(\hat{\phi}_{ij})}{\sum_i |\mu(\hat{\phi}_{ij})|} \qquad (3)$$

where $\sigma(\hat{\phi}_{ij})$ and $\mu(\hat{\phi}_{ij})$ are the standard deviation and mean of the jth identified mode shape at the ith DOF, $\hat{\phi}_{ij}$.

A comparison of the average 95% confidence bounds and the predicted changes as a result of damage for the mode shapes are shown (on a semilog scale) in Figure 11. Although many of the mode shapes un-
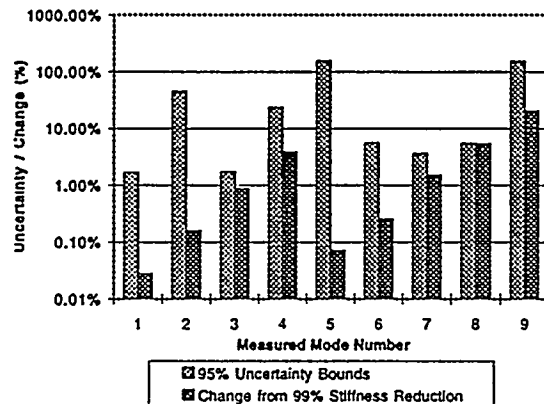

Figure 11. Comparison of Average Mode Shape Component 95% Confidence Bounds to Changes Predicted as a Result of Damage

dergo a significant (> 5%) average change, none of the mode shapes undergo an average change over all degrees of freedom that is larger than the 95% confidence bounds due to random variations in the measurements. Mode 8 is the only mode whose average change is near statistical significance. This figure only indicates the average change over all of the mode shape components, however, when in fact several of the mode shapes undergo a large localized change at particular DOF. The total number of DOF where the mode shape components undergo a change equal to or greater than the 95% confidence bounds is shown in Table 5. Mode

Table 5. Number of DOF for Each Mode Shape That Undergo Change Resulting from Damage >=95% Confidence Bounds.

Mode Number	Number of Mode Shape Components with Change > 95% Bound	Maximum ratio of component change to 95% Bound
1	0	0.069
2	0	0.016
3	9	2.521
4	0	0.982
5	0	0.002
6	1	1.048
7	5	2.955
8	6	5.431
9	1	1.361

8 has the component with the largest change. It is interesting to note that although mode shapes 3, 7, and 8 have average changes that are less than the average 95% uncertainty bound, they have 9, 5, and 6 individual components (out of 30 total) that undergo a significant change, respectively.

The statistical significance of changes to the mode shape curvature can be evaluated in a manner analogous to the analysis of the mode shapes. The most basic method is a direct, component-by-component comparison, as shown in Figure 12 for modes 3 and 7. In this case, mode 3 shows only slight changes in some of its curvature components, whereas mode 7 shows a large change in two of its curvature components. It should be noted that the curvatures shown in Figure 12 are the curvatures in the x-direction of the sensor configuration, which is parallel to the cross-members and perpendicular to the girders. Therefore, the curvatures of Figure 12 are not the second derivatives of the mode shapes shown in Figure 10 along the y-axis, but rather along the transverse direction.
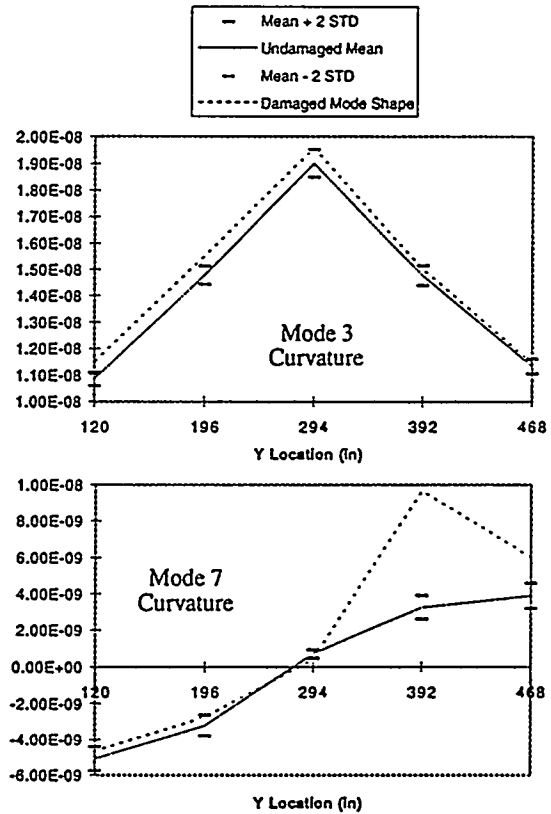

Figure 12. Comparison of Modes 3 and 7 Curvature Confidence Bounds and Predicted Change After Damage

Indicators that show the average uncertainty and change in curvature after damage were defined analogous to those defined for mode shapes in Eq. (2) and Eq. (3). A comparison of the average 95% confidence bounds and the predicted changes as a result of damage for the mode shape curvature components for each mode are shown in Figure 13. Although many of the mode shape curvatures undergo a significant (> 5%) average change, none of the mode shape curvatures undergoes an average change over all degrees of freedom that is larger than the 95% confidence bounds due to random variations in the measurements. Modes 3 and 8 are the only modes whose average curvature change is near statistical significance. This figure only indicates the average change over all of the mode shape curvature components, however, when in fact several of the mode shapes undergo a large localized curvature change at particular DOF. The total number of DOF where the mode shape components undergo a change equal to or greater than the 95% confidence bounds is shown in Table 6. Mode 7 has the individual component with the largest curvature change. It is interesting to note that although mode shape curvatures 3, 6, 7, 8 have average changes that are less than the average 95% uncertainty bound, they have 7, 3, 9 and 8 individual components that undergo a significant
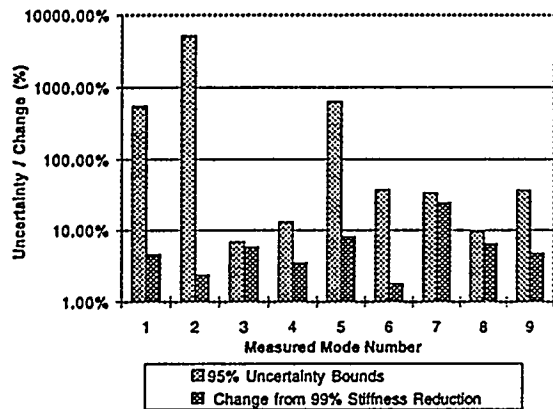
Figure 13. Comparison of Average Mode Shape Curvature Component 95% Confidence Bounds to Changes Predicted as a Result of Damage

Table 6. Number of DOF for Each Mode Shape Curvature That Undergo Change Resulting from Damage >=95% Confidence Bounds.

Mode Number	Number of Mode Curv. Components with Change > 95% Bound	Maximum ratio of component change to 95% Bound
1	0	0.207
2	0	0.011
3	7	2.552
4	0	0.858
5	0	0.866
6	3	2.124
7	9	9.929
8	8	5.248
9	0	0.901

change, respectively. The bottom line on the statistical analysis of the mode shape curvature changes is that over all their components, they generally do not exhibit a change larger than the 95% uncertainty bounds. However, individual components of certain mode shape curvatures exhibit changes that are much larger than the 95% uncertainty bounds, as shown for mode 7 in Figure 12. Therefore, individual components of the mode shape curvatures can be used for damage identification, but the analyst should compare the measured changes in curvature to the computed 95% uncertainty bounds to determine whether the observed changes in curvature are statistically significant.

CONCLUSION

Changes in basic damage indicators as a result of simulated damage were compared to variations in the indicators resulting from random variability in the measurements. The results demonstrate that modal frequency undergoes a statistically significant change as a result of the simulated damage, as do individual components of the mode shape and mode shape curvature. The average mode shape and average mode shape curvature undergo large changes in an absolute sense, but they also have much larger levels of uncertainty resulting from random variations in the measurements. The statistical significance of changes in the modal parameters could be used as criteria for "filtering" the modal parameters to perform a damage analysis in a selective manner. For example, perhaps only particular components of certain mode shapes should be used in damage analysis. The bottom line is that the statistical significance of changes in modal parameters, and not just the changes themselves, must be taken into account when using modal test results for damage identification. Future work will explore the use of these statistical confidence bounds for the enhancement of damage identification algorithms.

ACKNOWLEDGMENTS

REFERENCES

[1]   Doebling, S.W., Farrar, C.R., Prime, M.B., and Shevitz, D.W., "Damage Identification and Health Monitoring of Structural and Mechanical Systems From Changes in Their Vibration Characteristics: A Literature Review," Los Alamos National Laboratory report LA-13070-MS.

[2]   Toksoy, T. and Aktan, A.E., "Bridge-condition Assessment by Modal Flexibility," *Experimental Mechanics*, Vol. 34, pp. 271–278, 1994.

[3]   Hemez, F.M. and Farhat, C. "Structural Damage Detection via a Finite Element Model Updating Methodology," *Modal Analysis: The International Journal of Analytical and Experimental Modal Analysis*, Vol. 10, No. 3, 152–166, 1995.

[4]   Zimmerman, D.C. and Kaouk, M., "Structural Damage Detection Using a Minimum Rank Update Theory," *Journal of Vibration and Acoustics,* Vol. 116, pp. 222–230, 1994.

[5]   Doebling, S.W., "Damage Detection and Model Refinement Using Elemental Stiffness Perturbations with Constrained Connectivity," in *Proc. of the AIAA/ASME/AHS Adaptive Structures Forum,* pp. 360–370, AIAA-96-1307, 1996. Accepted and to appear in *AIAA Journal.*

[6]   Stubbs, N., Kim, J.-T., and Farrar, C.R., "Field Verification of a Nondestructive Damage Localization and Severity Estimation Algorithm," in *Proc. 13th International Modal Analysis Conference,* pp. 210–218, 1995.

[7]   Farrar, C.R., Doebling, S.W., Cornwell, P.J., and Straser, E.G., "Variability Of Modal Parameters Measured On The Alamosa Canyon Bridge," to appear in *Proc. of the 15th International Modal Analysis Conference,* Orlando, FL, February, 1997.

[8]   Allemang, R.J., "Vibrations: Experimental Modal Analysis," University of Cincinnati Class Notes, UC-SDRL-CN-20-263-663/664.

[9]   Shih, C.Y., Tsuei, Y.G., Allemang, R.J., Brown, D.L., "Complex Mode Indicator Function and Its Application to Spatial Domain Parameter Estimation," *Mechanical Systems and Signal Processing,* Vol. 2, No. 4, pp. 367-377, 1988.

[10]   Juang, J.N. and Pappa, R.S., "An Eigensystem Realization Algorithm for Modal Parameter Identification and Model Reduction," *Journal of Guidance, Control and Dynamics,* Vol. 8, No. 5, Sept.-Oct. 1985, pp. 620-627.

[11]   Pappa, R.S., Elliott, K.B., and Schenk, A., "Consistent-Mode Indicator for the Eigensystem Realization Algorithm," *Journal of Guidance, Control and Dynamics,* Vol. 16, No. 5, Sept.-Oct. 1993, pp. 852–858.

[12]   Bendat, J.S. and Piersol, A.G., *Engineering Applications of Correlation and Spectral Analysis,* John Wiley and Sons, New York, 1980, p. 274.

[13]   Press, W.H., Teukolsky, S.A., Vetterling, W.T., and Flannery, B.P., *Numerical Recipes in FORTRAN: The Art of Scientific Computing,* Second Edition, Cambridge Univ. Press, 1992, pp. 684-686.